JACS
JOURNAL OF THE AMERICAN CHEMICAL SOCIETY
pubs.acs.org/JACS
Article

Diels–Alder/Retro-Diels–Alder Reactions as Fold Altering Chemical Stimuli to Control the Self-Assembly of Aromatic Oligoamides

Louis Smal, François Kerff, Koen Robeyns, and Michael L. Singleton*

Cite This: https://doi.org/10.1021/jacs.5c14812
Read Online

ABSTRACT: Self-assembly of aromatic oligoamides into multihelical structures is a powerful strategy for developing complex and functional molecular architectures. As the hybridization process is directed by the folded state of the oligomers, inducing changes in the folding can be used to control the self-assembly. As one approach for this, Diels–Alder reactions on diazaanthracene monomers allow site-specific modification of aromatic oligoamides. The reaction leads to a bend in the monomer that, in turn, distorts the structure of the oligomer. Herein, we show that this strategy can be used to control the self-assembly of the oligomers. Using reversible Diels–Alder reactions allows switching between distinct folded states with different self-assembly preferences. This strategy can be applied during oligomer synthesis to prevent self-assembly or postsynthetically to disassemble multihelical structures. In complex systems containing multiple oligomers, we show that the modification can further be used to direct social versus narcissistic self-sorting, allowing for the switch between homomeric and heteromeric double helical assemblies.

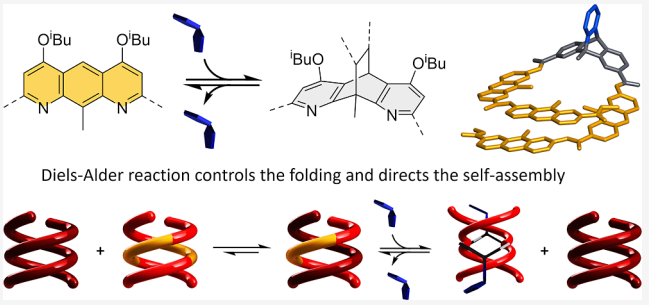

INTRODUCTION

The interplay between folding and self-assembly is central to the structure and function of complex biological systems and increasingly important in the design of synthetic materials.[1] In proteins, for example, folding of peptide sequences into ordered secondary and tertiary structures gives rise to well-defined tectons with distinct shapes and electrostatic potential surfaces, allowing for highly selective self-assembly between different complementary components.[2] As folding is an equilibrium process, these structures are subject to influences by their environment, chemical modification, or interactions with other molecules.[3] This allows regulation of their form, and in turn, their self-assembly. Such changes are crucial for the regulation of biological function, allowing proteins to switch between active and inactive states or adapt their assembly in response to external stimuli.[4] This method of structural control provides a compelling approach to develop synthetic systems that can similarly adapt or switch their self-assembly in a programmable manner.

Over the last decades, foldamers, synthetic oligomers that adopt stable, well-defined, higher-ordered structures in solution, have emerged as powerful scaffolds for mimicking aspects of biological folding.[5] Their ability to adopt predictable folded conformations enables the precise spatial positioning of functional groups on their surfaces. As a result, foldamers have attracted interest for a range of applications, including catalysis, molecular recognition, and biomedical applications.[6] Additionally, like for biomolecules, the functionalization combined with their large surface areas can allow for selective self-assembly, for example, into bundles[7] or cages,[8] through a combination of electrostatic interactions and solvophobic effects. The above applications and self-assembly generally rely on the idea of a single "static" conformation for functional group placement. While dynamic or stimuli-responsive folding behavior, such as helix to coil transitions or helicity inversions, is increasingly explored,[9] the ability to translate such behavior into control over self-assembly pathways is rare. Reversible switching between monomeric, homomeric, and heteromeric multistrand architectures remains a challenge.

This challenge is particularly relevant in the case of aromatic foldamers,[10] sequences composed of aromatic units as the main chain. In addition to self-assembly driven by interaction between exohedral functional groups, some of these sequences can also hybridize into double, triple, or even quadruple helices through strand intercalation, Figure 1a.[11] This process provides a route to significantly expand the structural and functional complexity accessible from relatively short sequences, with each strand contributing not only to the increased size of the assembly but also bringing distinct recognition or functional domains.

Received: August 26, 2025
Revised: January 20, 2026
Accepted: January 23, 2026

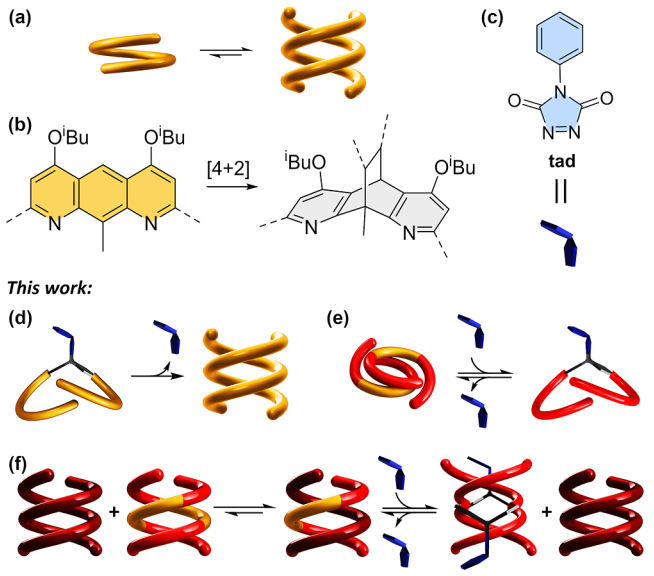

Figure 1. Schematic representations of (a) double helix formation through strand intercalation, (b) Diels–Alder modification of 1,8-diazaanthracene units, (c) Structure of 4-phenyl-1,2,4-triazoline-3,5-dione (**tad**) and cartoon representation colored in blue, and (d–f) overview of the directed structural transformations described in this work which allow (d) turning on self-assembly, (e) reversible tuning of the self-assembly properties, and (f) the multistate control and switching between homomeric and heteromeric assemblies.

Still, while hybridization represents a valuable design tool for aromatic foldamers, it can introduce synthetic challenges. The presence of multiple strands can block reactive sites, and hybridization of intermediates or their intercalation in longer oligomers can reduce the speed and efficiency of coupling reactions. In mixtures of oligomers, competing assembly pathways can reduce selectivity and make the outcome of self-assembly difficult to predict. For instance, selective formation of heterodouble helices remains difficult.[12] As a result, strategies that allow precise and reversible control over hybridization behavior are highly desirable.

To address this, a handful of methods have been described in the literature. Beyond changes in the medium, i.e., solvent polarity or pH,[13] guest binding[14] or changes in redox states[15] can also shift the equilibrium between single and double helical forms. Similarly, the use of N-protected tertiary amides can weaken folding propensity.[16] Subsequent deprotection can then induce folding, allowing self-assembly. More recently, photoresponsive units[17] and disulfide linkages[18] have been employed to control the composition of multihelical structures, enabling reversible switching between intra- and intermolecular duplex formation. Despite this growing toolbox, most approaches act peripherally or irreversibly. Few provide direct, reversible control of folding at the backbone level, particularly in the context of strand hybridization.

Recently, we demonstrated that 1,8-diazaanthracene (**A**) monomers can be selectively derivatized via Diels–Alder reaction to yield diazatriptycene (**T**) or iptycene units suitable for incorporation into aromatic oligoamide foldamers, Figure 1b.[19] This modification not only adds a bulky group to one face of the oligomer but also distorts its secondary structure by introducing a bend in the sequence. As this reduces the π-surface available for stabilizing multihelical structures, we reasoned that it could serve as an effective strategy for limiting multiple helix formation and exerting control over foldamer self-assembly.

In this work, we report a Diels–Alder/retro-Diels–Alder approach using 4-phenyl-1,2,4-triazoline-3,5-dione (**tad**), Figure 1c,[20] to reversibly modify aromatic oligoamides. The **tad** adducts can be introduced either during synthesis or postsynthetically to modulate oligomer folding and self-assembly behavior. It can then be cleanly removed in the presence of a sacrificial diene to restore the initial properties of the oligomer. In this sense, the **tad** group acts as a synthetic analogue of molecular chaperones, being able to disrupt the folded structures and selectively block key interaction surfaces. We show that this strategy not only allows control over single/double helical equilibria, but also that in complex mixtures of oligomers, it provides a method to selectively direct self-assembly between hetero- and homomeric double helices, Figure 1d–f.

RESULTS AND DISCUSSION

To study the effect of the Diels–Alder modification on self-assembly, sequences **1** and **2**, Figure 2, were chosen. Both of these oligomers self-assemble into highly stable double helices, with dimerization constants among the highest reported for this class of compound ($K_{dim} > 10^7$ in $CDCl_3$).[12b,21] With **1**, previous studies also showed that it could further weakly hybridize into triple helices, though this species was present only in small amount in solution.[12b] To demonstrate that Diels–Alder modification could prevent or limit self-assembly of these oligomers, the **A** monomer in the sequences were replaced by **T**, **M**, or **D** units, Figure 2, The Diels–Alder modifications lead to similar structural distortions in the monomers, Figure S1. However, for **T** and **M**, the 9,10-bridging groups are essentially an irreversible modification, making them valuable controls for looking at the effects on oligomer behavior. By contrast, with **D**, the **tad** unit undergoes readily reversible cycloadditions with anthracene derivatives,[20] and should allow reversible modulation of oligomer structure and behavior.

Blocking Self-Assembly of 1 through Control Over Oligomer Secondary Structure

As an initial confirmation that the Diels–Alder modification could limit the formation of multihelical structures, pentamers **1-T** and **1-D**, Figure 2, were synthesized. The crystal structure of **1-T**, Figure 3a,b, shows the oligomer folded into a distorted single helical conformation as a result of the ~ 130° bend introduced by the central **T** unit. Despite this, deviation in the torsion angles around the amides allows both ends of the sequence to stack, with the terminal **A** moieties almost completely overlapping. Attempts to crystallize **1-D** were unsuccessful. Although the oligomer is stable in solution at room temperature for several days, slow retro-Diels–Alder reaction occurs over extended periods, yielding crystals of a triple-helical form of **1**, Figure S2, that forms only weakly in solution. Still, given the analogous geometries of the **T** and **D** units, and the supporting solution data (see below), **1-D** is expected to adopt the same folded conformation as **1-T**.

In $CDCl_3$, the ^{1}H NMR spectra of both **1-T** and **1-D** are highly similar, Figure 3c,d. Each oligomer displays only two amide resonances indicating rapid fluxional processes, i.e. P/M interconversion and **tad** group flipping, that render both ends equivalent by ^{1}H NMR. Varying the concentration of the oligomers from 1 to 10 mM, Figures S3 and S4, does not lead

https://doi.org/10.1021/jacs.5c14812
J. Am. Chem. Soc. XXXX, XXX, XXX–XXX

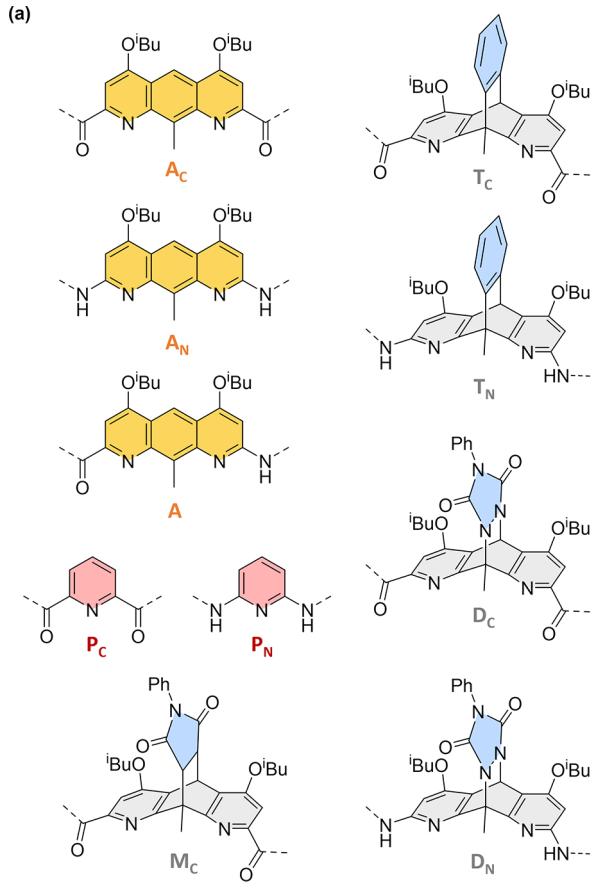

(b)

	Sequences		
1	MeO-AAA$_C$AA-OMe	2	Boc-P$_N$P$_C$P$_N$A$_C$P$_N$P$_C$P$_N$-Boc
1-T	MeO-AAT$_C$AA-OMe	2-T	Boc-P$_N$P$_C$P$_N$T$_C$P$_N$P$_C$P$_N$-Boc
1-D	MeO-AAD$_C$AA-OMe	2-M	Boc-P$_N$P$_C$P$_N$M$_C$P$_N$P$_C$P$_N$-Boc
		2-D	Boc-P$_N$P$_C$P$_N$D$_C$P$_N$P$_C$P$_N$-Boc
3	Boc-P$_N$P$_C$A$_N$P$_C$P$_N$-Boc		
3-T	Boc-P$_N$P$_C$T$_N$P$_C$P$_N$-Boc	4	Boc-P$_N$P$_C$P$_N$P$_C$P$_N$P$_C$P$_N$-Boc
3-D	Boc-P$_N$P$_C$D$_N$P$_C$P$_N$-Boc		

Figure 2. Color-coded formulas and associated abbreviations for the (a) aromatic units and (b) oligoamide sequences **1**−**4** used in this study. The colors shown correspond to the colors used in the X-ray structures and cartoon representations.

to the appearance of new resonances, nor to significant chemical shift changes, suggesting either highly stable self-assembled structures, which is unlikely given the high fluxionality, or purely single-helical forms as seen in the X-ray structure of **1-T**, Figure 3a,b.

Consistent with the latter, ^{1}H−^{1}H NOESY analysis of both **1-T** and **1-D**, Figures S5 and S6, showed through−space correlations between the methyl ester group and the 10-position proton of the nonterminal **A** unit, in agreement with the close contacts observed in the solid-state structure of **1-T**, Figure 3b. Qualitative comparison of the ^{1}H chemical shifts observed for **1-T** and **1-D** further supports their single helical nature in solution, Figure S7.

In multihelical aromatic oligoamides, the resonances are typically shifted upfield relative to short units or single helical structures, owing to increased aromatic stacking and the corresponding ring current effect. For instance, in double-helical **1**, the 10-position protons of the **A** units appear at 7.9

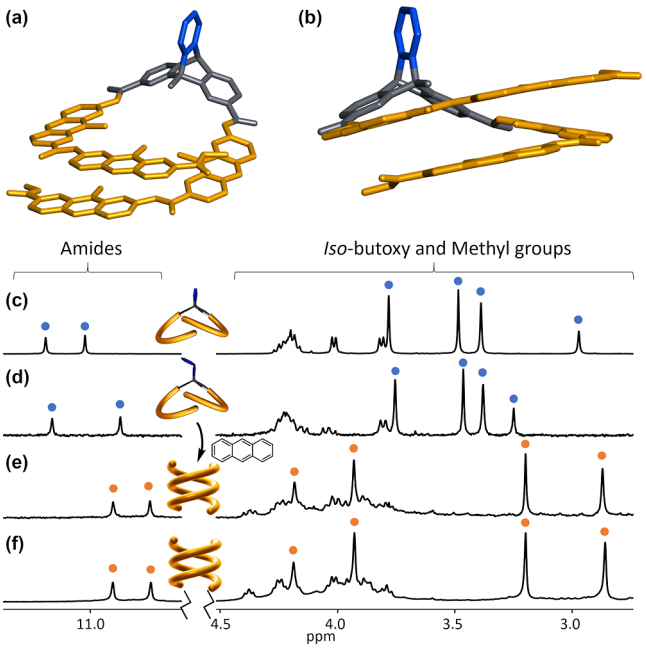

Figure 3. (a,b) Views of the crystal structure of **1-T**. Side-chains and included solvent molecules have been removed for clarity. (c−f) Parts of the 400 MHz ^{1}H NMR spectra in $CDCl_3$ solutions at 293 K of (c) **1-T** [10 mM], (d) **1-D** [1 mM], (e) **1-D** [10 mM] after the addition of an excess of anthracene and heating, and (f) **1** [10 mM]. The indicative ^{1}H resonances are indicated with blue circles for **1-T** and **1-D** and orange circles for **1**.

and 8.5 ppm, whereas in the starting $\mathbf{A}_2$ dimer or in an **ATA** trimer,[19] where no stacking is present, the corresponding resonances are found at 8.9 and 9.0 ppm, respectively. In both **1-T** and **1-D**, the 10-position resonances of the terminal and nonterminal **A** units occur at 8.7 and 9.1 ppm respectively, consistent with stacking interactions only for the terminal **A** units, as seen in the crystal structure of **1-T**. Thus, in solution, as in the solid-state, both **1-T** and **1-D** are single helical and show no signs of self-assembly into higher-ordered structures, highlighting the blocking effect of the Diels−Alder modification.

Importantly, removal of the Diels−Alder modification in **1-D**, restores the parent oligomer structure (**1**), allowing it to self-assemble. This can be achieved cleanly by gently heating a chloroform solution of **1-D** in the presence of anthracene as a **tad** scavenger, transferring the 9,10-bridging group from the oligomer to the added anthracene and restoring the planar structure of the central monomer. When followed by ^{1}H NMR, Figures 3e and S8, the resonances corresponding to **1-D** completely disappear, and two new sets of resonances appear corresponding to oligomer **1** and the **tad** adduct of anthracene. The chemical shifts observed for the former match perfectly with the spectrum of the reported double helical **1**, Figure 3f, confirming that **tad** removal triggers self-assembly.

Effect of Diels−Alder Modification on Longer Oligomers

Blocking the self-assembly becomes more complex for longer oligomers. Because **2** spans two full helical turns, the greater potential for strand intercalation can allow hybridization into multihelical structures after Diels−Alder modification, leading to distinct behaviors depending on the exact distortion introduced. To study this, sequences **2-T**, **2-D**, and **2-M**, Figure 2, were synthesized.

https://doi.org/10.1021/jacs.5c14812
J. Am. Chem. Soc. XXXX, XXX, XXX−XXX

Indeed, the X-ray structures of all three oligomers show that double helices can still form, Figure 4a–d, albeit with markedly different geometries. For **2-T**, the bridging benzene group imposes a strong steric constraint perpendicular to the monomer plane. The pyridine arms of the oligomer cannot stack above the central monomer and the oligomer adopts a unique mixed-fold topology where one-half forms a conventional double helix, while the other half flips outward before intertwining with its partner, placing the two helical axes at roughly 90° to each other. Interestingly, the correctly folded side of the oligomer is highly extended, leading to a minor and major groove with interstrand separations of ∼ 3.5 and 7 Å, respectively. The larger spacing allows intercalation with the corresponding section of a neighboring double helix in the crystal lattice, resulting in a tetrameric structure in the solid-state, Figure 4b.

Both **2-M** and **2-D** hybridize into more conventional double helices, Figure 4c,d, reinforced by hydrogen bonding between the terminal pyridine endocyclic nitrogens and the carbamate N–Hs. Still, there are noticeable structural distortions resulting from the Diels–Alder modified monomers. The 9,10-bridging groups of the **M** or **D** units are oriented toward the same side of the helix forcing the pyridines of the partner strand to stack on top of these groups. This disrupts the compact structure normally seen in double helical assemblies and results in a clear bend (∼135°) in the helical axis. Aside from minor differences in stacking arrangements and the 9,10-bridging group, the two assemblies, **2-M** and **2-D**, are essentially structurally equivalent.

Because two distinct helix topologies were identified within the series (**2-T** vs **2-M**/**2-D**), the possibility that **2-D** might also access a **2-T** like arrangement was examined computationally. Semiempirical optimizations at the PM6-D3H4 level[22] were carried out on **2-D** in both possible geometries, Figure S9. The **2-M**/**2-D** type double helix was predicted to be lower in energy by 6.8 kcal mol^{-1}, suggesting that the **2-T** type arrangement is significantly less favorable for **2-D**.

To determine whether similar hybridization occurs in solution, variable concentration studies in $CDCl_3$ were performed with **2-T**, **2-M**, and **2-D**, Figures 5a–g and S10–S14. The behavior varies significantly between the three oligomers.

2-T generally behaves as a single helix. At 1 mM, three amide resonances are observed for **2-T**, Figures 5a and S10, consistent with a flexible single helical structure, similar to what was observed for **1-T**. Increasing the concentration to 10 mM, Figure 5b, leads only to a broadening of the resonances and minor changes in chemical shift but no new resonances appear. Even at concentrations up to 40 mM, no new species are observed, indicating that discrete double helix formation with **2-T** is unfavorable in solution. DOSY studies on a 1:1 mixture of **2-T** with double helical **2**, Figure S15, also show a larger diffusion coefficient for **2-T**, and thus smaller solvodynamic radius, further supporting its single helical nature in solution.

Both **2-M** and **2-D** show more pronounced concentration dependent changes. The ^1H NMR spectrum of **2-M** at 1 mM in water saturated $CDCl_3$,[23] Figure 5c, shows six amide resonances between 10 and 11 ppm consistent with the asymmetric nature of the central monomer. At higher concentrations, a second set of broad resonances appears and increases in relative intensity with concentration, Figures 5d and S11. Upon cooling to 0 °C, these resonances sharpen,

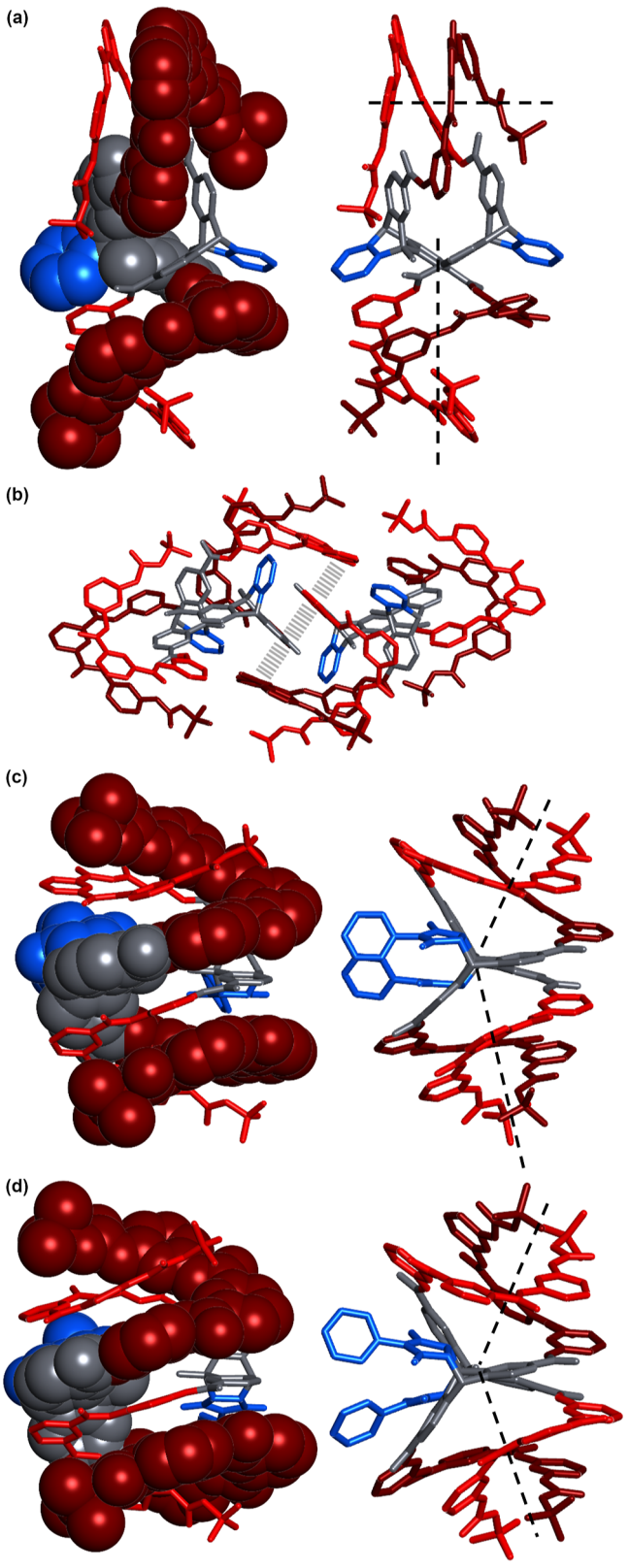

Figure 4. Views of the crystal structure of (a) **2-T**, (b) the tetrameric **2-T** structure observed in the solid state, (c) **2-M**, and (d) **2-D**. Side-chains and included solvent molecules have been removed for clarity. Dashed lines in (a,c, and d, right) show the relative orientation of the double helical axes on either side of the structure. Potential π-stacking interactions are shown with dashed bars in (b).

https://doi.org/10.1021/jacs.5c14812
J. Am. Chem. Soc. XXXX, XXX, XXX–XXX

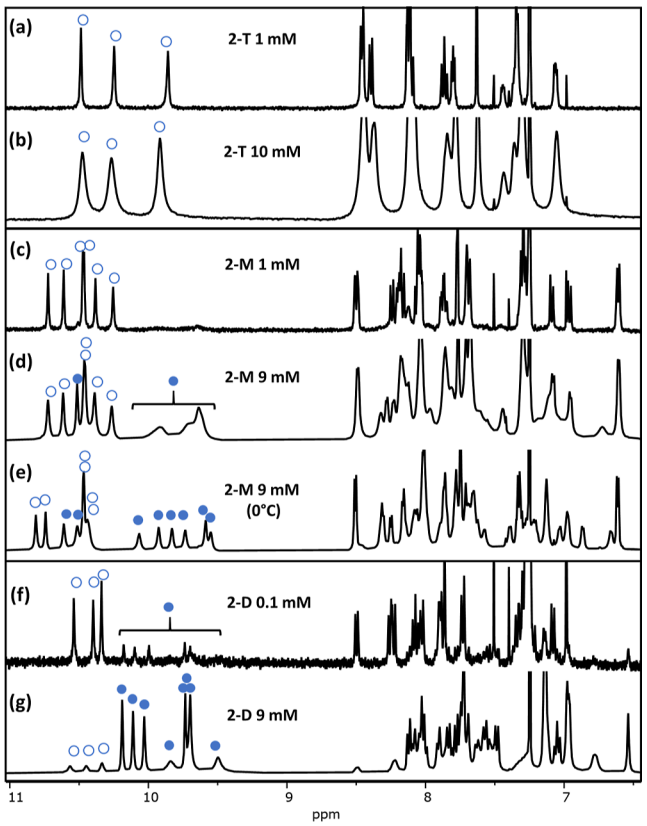

Figure 5. Portions of the ^{1}H NMR spectra showing the amide, carbamate and aromatic resonances in $CDCl_3$ for (a) **2-T** [1 mM] and (b) **2-T** [10 mM] and in water saturated $CDCl_3$ for (c) **2-M** [1 mM], (d) **2-M** [9 mM], (e) **2-M** [9 mM] at 0 °C, (f) **2-D** [0.1 mM], and (g) **2-D** [9 mM]. Resonances for the monomeric species are indicated with empty blue circles and distinct resonances for the duplexes are indicated with filled blue circles.

and eight resonances corresponding to the amide and carbamate N−Hs can be observed, Figures 5e and S16.

Similar changes are observed for **2-D**, except that the second species can be observed even at low concentration, Figures 5f and S14. At 0.1 mM, the major species displays three amide resonances, again indicative of a highly fluxional single helical form, as seen for **1-D**. At higher concentrations, Figure 5g, the second set of resonances increases in intensity and eight resonances corresponding to the amide and carbamate N−Hs can be observed, suggesting lower symmetry and a loss of fluxionality. Such changes could be expected with double helix formation, where flipping of the **tad** group and P/M helicity inversion would be hindered.

Several pieces of evidence support that the two species observed for **2-M** and **2-D** result from an equilibrium between single and double helical forms. First, for both oligomers, the quantity of the different species at each concentration fit well to simple dimerization isotherms, Figures S17 and S18, with K_{dim} = 71 for **2-M** and $K_{dim} = 1.6 \times 10^3$ for **2-D**, four to six orders of magnitude lower than the parent oligomer, **2**. HRMS evidence also supports the presence of both monomeric and dimeric species, Figures S19−S22. Finally, interstrand correlations, Figures 6 and S23−S27, can be observed by ^{1}H−^{1}H NOESY between the carbamate N−H resonances and the two N−H (carbamate and amide) of the terminal pyridine units of the neighboring strand, consistent with the hydrogen-bonding pattern observed in the solid-state structures. Correlations are also observed between the endohedral methyl groups and several of the amide N−Hs, further supporting the close interstrand packing seen in the double helical structures.

Together, these results show that although the Diels−Alder modifications consistently suppress self-assembly, longer sequences can still form duplexes. With **tad**, this opens the possibility to not only modulate these interactions but also to postsynthetically switch between different self-assembled structures.

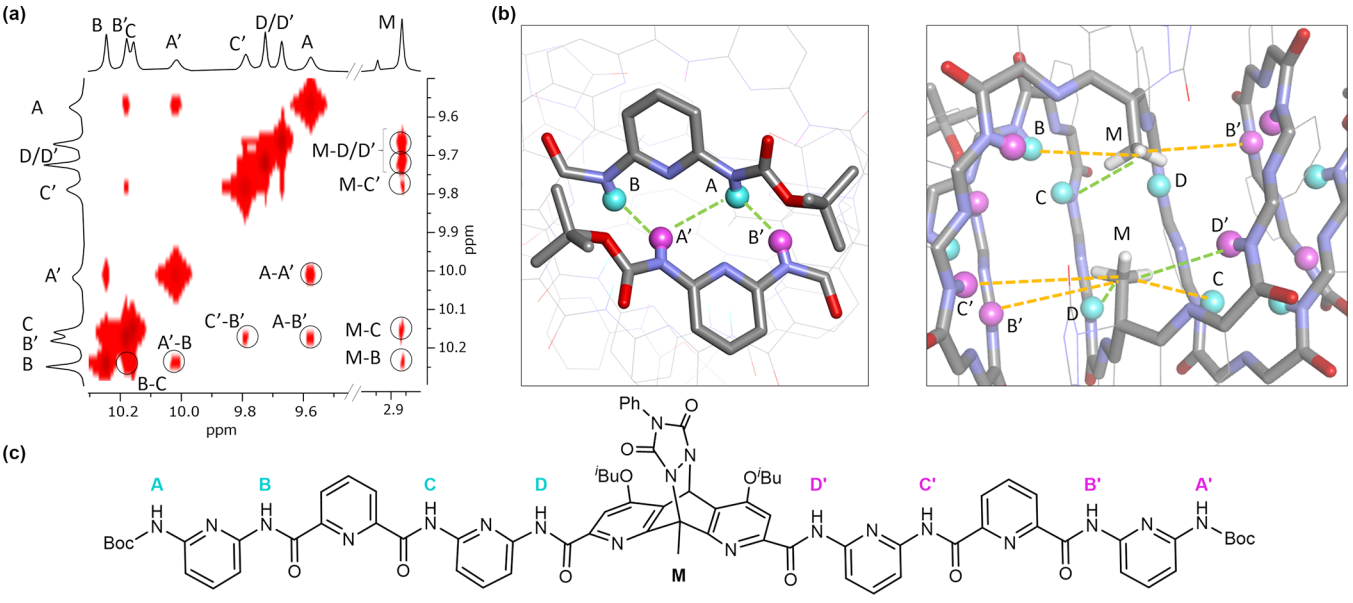

Figure 6. (a) Portions of the ^{1}H−^{1}H NOESY spectrum of **2-D** at 0 °C in water saturated $CDCl_3$ showing the amide and methyl group correlations. Threshold level for the methyl region is set lower than for the amides to observe these weaker correlations. (b) Portions of the X-ray structure of **2-D** showing close contacts. Amide and carbamate protons are shown as blue or purple spheres. Dashed lines indicate H−H distances of <3 Å (Green) or <4 Å (Yellow). (c) Structure of **2-D** showing the positions of the labeled resonances in (a).

https://doi.org/10.1021/jacs.5c14812
J. Am. Chem. Soc. XXXX, XXX, XXX−XXX

Postsynthetic Diels–Alder Modification

Guided by this possibility, we next looked at whether the **tad** Diels–Alder modification could be performed directly on the oligomers to control their structure. Such, postsynthetic modification of aromatic oligoamides, beyond side-chain reactions, is rare.[24] In oligomer **1**, addition of **tad** leads to complex mixtures by ^{1}H NMR due to multiple reactive sites. However, oligomers **2**[21] and **3**, Figure 2, each containing a single **A** unit, should more easily undergo clean reversible reactions with **tad**.

With oligomer **2**, the high dimerization constant and compact structure lead to slow reaction with **tad**, requiring long reaction times or a large excess of **tad** to achieve full conversion of the oligomer. Still, after addition of 5 equiv of **tad** at 10 mM in $CDCl_3$, complete disappearance of the resonances for **2** can be seen after 24 h, Figure 7a,b, and S28.

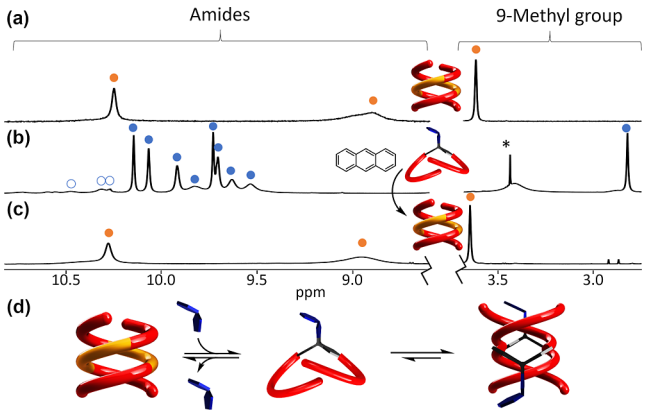

Figure 7. Parts of the 400 MHz ^{1}H NMR spectra in $CDCl_3$ solutions at 293 K of (a) **2** [5 mM], (b) **2** [10 mM] after the addition of **tad** (**2-D**), (c) the resulting product [10 mM] after addition of an excess of 10 equiv of anthracene and heating (**2**) and (d) cartoon scheme of the proposed equilibrium present with **2-D**. The ^{1}H resonances of the different species are indicated with orange circles (**2**) and empty (**2-D**) or filled ((**2-D**)$_2$) blue circles. Methanol resonance is indicated with *.

These are replaced by the collection of resonances corresponding to **2-D**, confirming the Diels–Alder modification of the oligomer. Transfer of the **tad** group to the sacrificial diene restores the resonances for **2**, Figure 7c, demonstrating complete and reversible structural control with the Diels–Alder approach and allowing switching between two duplex forms, Figure 7d.

Oligomer **3** aggregates weakly. In the solid-state, **3** forms a partially stacked duplex stabilized by interstrand hydrogen bonding, Figure 8a. Specific concentration dependent shifts and ^{1}H–^{1}H NOESY contacts, Figures 8c and S29–S30 indicate aggregation also occurs in $CDCl_3$. No such behavior is observed for **3 T**, Figures 8b,d and S31, confirming that the Diels–Alder modification limits self-assembly. With **tad**, this control can be exerted postsynthetically in a reversible fashion.

Addition of **tad** to **3** in $CDCl_3$ cleanly affords Diels–Alder adduct **3-D** by ^{1}H NMR, Figures 8c,e and S32, as evidenced by the disappearance of the 9-position methyl resonance of the **A** unit (3.2 ppm) and appearance of a new upfield resonance at 2.7 ppm for the same protons in **3-D**. Similar to **3-T**, **3-D** shows no concentration dependent shifts from 1 to 10 mM in $CDCl_3$, consistent with limited aggregation, Figure S33. Like

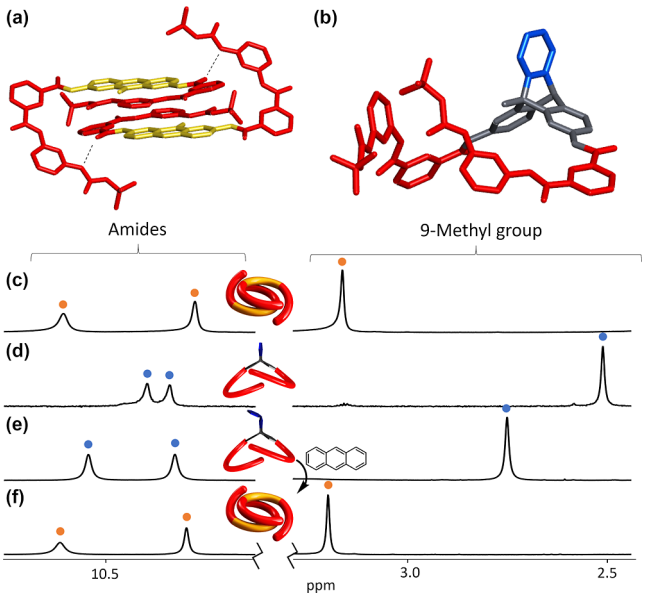

Figure 8. Views of the crystal structure of (a) **3** and (b) **3-T**. Side-chains and included solvent molecules have been removed for clarity. Parts of the 400 MHz ^{1}H NMR spectra in $CDCl_3$ solutions at 293 K of (c) **3** [10 mM], (d) **3-T** [1 mM], (e) **3** [10 mM] after the addition of **tad** (**3-D**), and (f) the resulting product [10 mM] after the addition of an excess of 10 equiv of anthracene and heating (**3**). The ^{1}H resonances of the different species are indicated with orange circles (**3**) and blue circles (**3-T** and **3-D**).

for **2-D**, heating **3-D** in the presence of anthracene also allows full reversion to the initial oligomer **3**, Figure 8f.

Folding Induced Switching between Hetero- and Homodouble Helices

We next asked whether the Diels–Alder induced structural changes could be used not only to control self-assembly of single sequences, but also to direct the assembly pathways in mixtures, Figure 9a. During this work, we serendipitously discovered that pyridine heptamer **4**[25] forms highly stable heterodouble helices with **2**. At 5 mM in $CDCl_3$, **4** exists as a mixture of single and double helices, Figure 9b, (K_{dim} = ~ 180 at 20 °C). Upon addition of one equivalent of **2**, the amide resonances of **4**, Figures 9b,d and S34, disappear almost completely and eight new resonances between 8.9 and 10.1 ppm appear, Figure 9d, corresponding to the amide and carbamate N–H protons in the heteroduplex **2·4**, Figure S35.

In the solid-state, **2·4** adopts a symmetric double helix, Figure 9g, similar to the homodimer of **2**, (**2**)$_2$. Close contacts between the terminal pyridine endocyclic nitrogen and carbamate N–H (N–N distances 3–3.2 Å) on each strand allow for hydrogen bonding pairs on both ends of the duplex. NOESY correlations between the 9-position methyl group on the central monomer of **2** and the amide N–Hs of **4** confirm that a similar arrangement persists in solution, Figure S36. The heterodouble helix composition was further supported by HRMS, Figure S37. Based on the estimated or known dimerization constants for **2** and **4** (>10^7 and 180 respectively at 20 °C),[21,25] the overall observed equilibrium constant for (**2**)$_2$ + (**4**)$_2$ → 2(**2·4**) is calculated to be > 5 × 10^3. This gives a K_{dim} for **2** + **4** → **2·4** of at least 10^6.

Addition of **tad** to a solution of **2·4** leads to complete disappearance of the heterodouble helix resonances in the ^{1}H NMR spectrum, Figures 9e, S38 and S39. These are replaced

https://doi.org/10.1021/jacs.5c14812
J. Am. Chem. Soc. XXXX, XXX, XXX–XXX

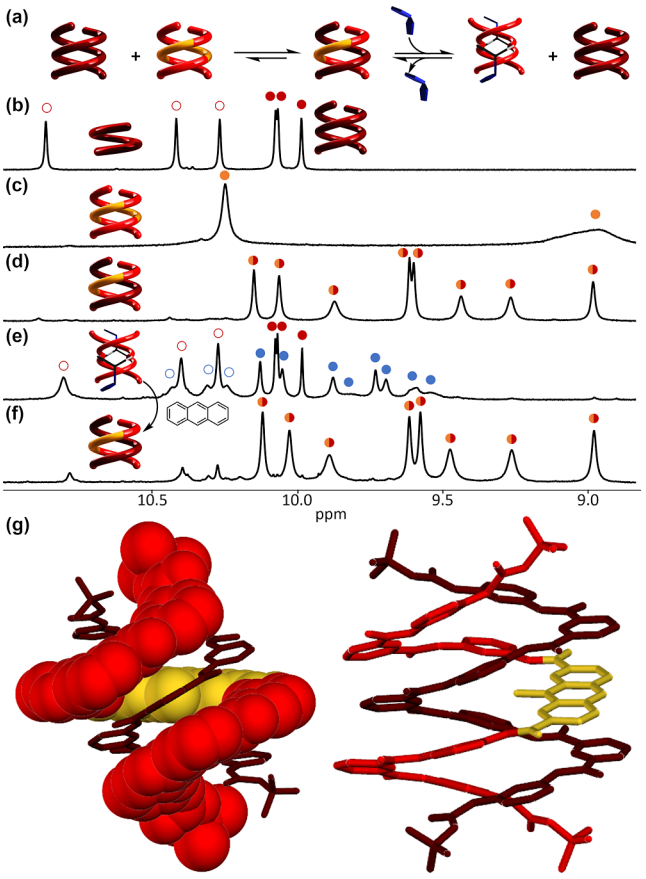

Figure 9. (a) Schematic cartoon of the three-state exchange process between homo- and hetero double helices using the Diels–Alder modification. Amide region of the 400 MHz ^{1}H NMR spectra in $CDCl_3$ solutions at 293 K of (b) **4** [5 mM], (c) $\mathbf{2}_2$ [5 mM], (d) **2·4** [5 mM], (e) **2·4** [5 mM] after the addition of **tad** (**4**+**2-D**), and (f) the resulting product [5 mM] after addition of 10 equiv of anthracene and heating. The ^{1}H resonances are indicated with empty (**4**) or filled ($\mathbf{4}_2$) red circles, orange circles ($\mathbf{2}_2$), red/orange circles (**2·4**), and empty (**2-D**) or filled ($(\mathbf{2\text{-}D})_2$) blue circles. (g) Views of the crystal structure of the hetero double helix (**2·4**). Side-chains and included solvent molecules have been removed for clarity.

by the resonances corresponding to single and double helical **4** and the monomeric and duplex forms of **2-D**. In essence, the **tad** modification leads to a switch from social to narcissistic self-sorting, driving the disassembly of the heteroduplex **2·4** and formation of the respective homomeric assemblies, $(\mathbf{2\text{-}D})_2$ and $\mathbf{4}_2$. Performing the retro-Diels–Alder reaction reverses this process. Upon heating in the presence of anthracene, the resonances corresponding to the heterodimeric **2·4** reappear, Figure 8f. Minor differences in some resonances remain, which is attributed to small variations in water content of the samples and the resulting influence on the oligomer behavior,[25,26] Figures S40–S42. Consistent with this, spectra recorded in DMSO-d_6, where the water effects are eliminated, show clean and unambiguous transition between the different states, Figure S39, confirming that the Diels–Alder modification with **tad** not only functions as a reversible trigger for structural reorganization in oligomer mixtures, but also enables controlled switching between distinct self-assembly states.

CONCLUSIONS

In summary, we have described a Diels–Alder/retro-Diels–Alder strategy based on **tad** and diazaanthracene monomers that gives multiple levels of control over the self-assembly of aromatic oligoamide foldamers into multihelical architectures. The Diels–Alder modification leads to changes in the folded structures, which in turn alter their interaction with other oligomers. The **tad** adduct can be incorporated during the synthesis of the oligomers, as in **1-D**, where it acts as a protecting group to prevent premature self-assembly. Subsequent addition of a sacrificial diene, like anthracene, allows transfer of the **tad** group from the oligomer and triggers the onset of self-assembly.

This strategy is also compatible with postsynthetic modification, as shown with oligomers **2** and **3**, allowing to modify their three-dimensional structure and control their self-assembly properties. The Diels–Alder modification inhibits or substantially decreases duplex formation by several orders of magnitude relative to the parent oligomers. Nevertheless, double helix formation can be possible in longer sequences, leading to unique structures, as seen in the solid-state for **2-T**, **2-M** and **2-D**, and providing new design possibilities for assemblies of aromatic oligoamides.

We further showed that **tad** modification can be used to direct homomeric versus heteromeric assembly formation. **2** forms highly stable heterodouble helices with **4**. Reaction of **tad** with the heteroduplex **2·4** leads to disassembly, allowing **4** and **2-D** to form their respective homoduplexes. Taking together the heterodouble helix formation and **tad** reactivity, this gives a controlled multistate exchange process for oligomer assembly where the **tad** modification serves as a reversible trigger for structural reorganization between two states. This dynamic switching mechanism not only highlights the tunability of the oligomer self-assembly, but also provides an effective strategy for controlling supramolecular architectures of aromatic oligoamides. While broader generalization of this approach will require further studies, the present system establishes a versatile platform for adaptive foldamer assemblies with potential applications in responsive materials, molecular recognition, and information storage.

ASSOCIATED CONTENT

Supporting Information

The Supporting Information is available free of charge at https://pubs.acs.org/doi/10.1021/jacs.5c14812.

The electronic Supporting Information contains complete synthetic and experimental procedures, additional NMR studies, and complete characterization data (PDF)

Accession Codes

Deposition Numbers 2480304–2480311 and 2514227 contain the supplementary crystallographic data for this paper. These data can be obtained free of charge via the joint Cambridge Crystallographic Data Centre (CCDC) and Fachinformationszentrum Karlsruhe Access Structures service.

AUTHOR INFORMATION

Corresponding Author

Michael L. Singleton – *Molecular Chemistry, Materials and Catalysis Division, Institute of Condensed Matter and Nanosciences, Université catholique de Louvain, Louvain-la-*

https://doi.org/10.1021/jacs.5c14812
J. Am. Chem. Soc. XXXX, XXX, XXX–XXX

Neuve 1348, Belgium; orcid.org/0000-0002-4018-9595; Email: m.singleton@uclouvain.be

Authors

Louis Smal − *Molecular Chemistry, Materials and Catalysis Division, Institute of Condensed Matter and Nanosciences, Université catholique de Louvain, Louvain-la-Neuve 1348, Belgium*

François Kerff − *Molecular Chemistry, Materials and Catalysis Division, Institute of Condensed Matter and Nanosciences, Université catholique de Louvain, Louvain-la-Neuve 1348, Belgium*

Koen Robeyns − *Molecular Chemistry, Materials and Catalysis Division, Institute of Condensed Matter and Nanosciences, Université catholique de Louvain, Louvain-la-Neuve 1348, Belgium;* orcid.org/0000-0002-4763-4217

Complete contact information is available at: https://pubs.acs.org/10.1021/jacs.5c14812

Author Contributions

The manuscript was written through contributions of all authors. All authors have given approval to the final version of the manuscript.

Notes

The authors declare no competing financial interest.

■ ACKNOWLEDGMENTS

This work was supported in part through support from the Fédération Wallonie Bruxelles, through the "Actions de Recherche Concertées" (ARC16/21-074-Slidenet, ARC24/29-139-Reacsurf) and FNRS CDR J.0168.22. L.S. and F.K. were supported through doctoral fellowships from the Fonds de la Recherche Scientifique−FNRS (FNRS-FRIA). We also thank Dr. Gabriella Barozzino for help with NMR measurements.

■ REFERENCES

(1) (a) Li, Z.; Cai, B.; Yang, W.; Chen, C.-L. Hierarchical nanomaterials assembled from peptoids and other sequence-defined synthetic polymers. *Chem. Rev.* **2021**, *121* (22), 14031−14087. (b) McMullen, A.; Muñoz Basagoiti, M.; Zeravcic, Z.; Brujic, J. Self-assembly of emulsion droplets through programmable folding. *Nature* **2022**, *610* (7932), 502−506. (c) Ni, R.; Abeln, S.; Schor, M.; Cohen Stuart, M. A.; Bolhuis, P. G. Interplay between folding and assembly of fibril-forming polypeptides. *Phys. Rev. Lett.* **2013**, *111* (5), 058101. (d) Maffeis, V.; Heuberger, L.; Nikoletić, A.; Schoenenberger, C.-A.; Palivan, C. G. Synthetic cells revisited: artificial cell construction using polymeric building blocks. *Adv. Sci.* **2024**, *11* (8), 2305837. (e) Wang, S.; Favor, A.; Kibler, R. D.; Lubner, J. M.; Borst, A. J.; Coudray, N.; Redler, R. L.; Chiang, H. T.; Sheffler, W.; Hsia, Y.; Bethel, N. P.; Li, Z.; Ekiert, D. C.; Bhabha, G.; Pozzo, L. D.; Baker, D. Bond-centric modular design of protein assemblies. *Nat. Mater.* **2025**, *24*, 1644. (f) Rankovic, S.; Carr, K. D.; Decarreau, J.; Skotheim, R.; Kibler, R. D.; Ols, S.; Lee, S.; Chun, J.-H.; Tooley, M. R.; Dauparas, J.; Eisenach, H. E.; Glögl, M.; Weidle, C.; Borst, A. J.; Baker, D.; King, N. P. Computational design of bifaceted protein nanomaterials. *Nat. Mater.* **2025**, *24*, 1635. (g) Heo, J.-M.; Park, J.; Kim, J.-M. Retro Diels-Alder-triggered self-assembly of a polymerizable macrocyclic diacetylene. *Org. Biomol. Chem.* **2023**, *21*, 6302−6306. (h) Park, J.; Heo, J.-M.; Seong, S.; Noh, J.; Kim, J.-M. Self-assembly using a retro Diels-Alder reaction. *Nat. Commun.* **2021**, *12*, 4207.

(2) (a) Raymond, D. M.; Nilsson, B. L. Multicomponent peptide assemblies. *Chem. Soc. Rev.* **2018**, *47* (10), 3659−3720. (b) Lou, S.; Wang, X.; Yu, Z.; Shi, L. Peptide tectonics: encoded structural complementarity dictates programmable self-assembly. *Adv. Sci.* **2019**, *6* (13), 1802043. (c) Valéry, C.; Pandey, R.; Gerrard, J. A. Protein β-interfaces as a generic source of native peptide tectons. *Chem. Commun.* **2013**, *49* (27), 2825−2827. (d) Li, Y.; Tian, R.; Shi, H.; Xu, J.; Wang, T.; Liu, J. Protein assembly: Controllable design strategies and applications in biology. *Aggregate* **2023**, *4*, No. e317.

(3) (a) Devi, S.; Chaturvedi, M.; Fatima, S.; Priya, S. Environmental factors modulating protein conformations and their role in protein aggregation diseases. *Toxicology* **2022**, *465*, 153049. (b) Del Giudice, A.; Del Giudice, D.; Spatola, E.; Alemanno, V.; Galantini, L.; Di Stefano, S. An albumin unfolding and refolding cycle induced by a time-controlled pH jump. *Org. Biomol. Chem.* **2024**, *23* (1), 118−125. (c) Clarkson, B. R.; Schön, A.; Freire, E. Conformational stability and self-association equilibrium in biologics. *Drug Discov Today* **2016**, *21* (2), 342−347.

(4) Kim, A. K.; Porter, L. L. Functional and regulatory roles of fold-switching proteins. *Structure* **2021**, *29* (1), 6−14.

(5) (a) Goodman, C. M.; Choi, S.; Shandler, S.; DeGrado, W. F. Foldamers as versatile frameworks for the design and evolution of function. *Nat. Chem. Biol.* **2007**, *3*, 252−262. (b) Guichard, G.; Huc, I. Synthetic foldamers. *Chem. Commun.* **2011**, *47* (21), 5933−5941. (c) Hill, D. J.; Mio, M. J.; Prince, R. B.; Hughes, T. S.; Moore, J. S. A field guide to foldamers. *Chem. Rev.* **2001**, *101* (12), 3893−4012. (d) Hecht, S.; Huc, I. *Foldamers: Structure, Properties, and Applications*; Wiley-VCH, 2007. (e) Gellman, S. H. Foldamers: a manifesto. *Acc. Chem. Res.* **1998**, *31* (4), 173−180. (f) Yashima, E.; Ousaka, N.; Taura, D.; Shimomura, K.; Ikai, T.; Maeda, K. Supramolecular helical systems: helical assemblies of small molecules, foldamers, and polymers with chiral amplification and their functions. *Chem. Rev.* **2016**, *116* (22), 13752−13990. (g) Arrata, I.; Grison, C. M.; Coubrough, H. M.; Prabhakaran, P.; Little, M. A.; Tomlinson, D. C.; Webb, M. E.; Wilson, A. J. Control of conformation in α-helix mimicking aromatic oligoamide foldamers through interactions between adjacent side-chains. *Org. Biomol. Chem.* **2019**, *17*, 3861−3867.

(6) (a) Lin, Q.; Lan, H.; Ma, C.; Stendall, R. T.; Shankland, K.; Musgrave, R. A.; Horton, P. N.; Baldauf, C.; Hofmann, H.-J.; Butts, C. P.; Müller, M. M.; Cobb, A. J. A. Crystal structure and NMR of an α,δ-peptide foldamer helix shows side-chains are well placed for bifunctional catalysis: application as a minimalist aldolase mimic. *Angew. Chem., Int. Ed.* **2023**, *62* (36), No. e202305326. (b) Bécart, D.; Diemer, V.; Salaün, A.; Oiarbide, M.; Nelli, Y. R.; Kauffmann, B.; Fischer, L.; Palomo, C.; Guichard, G. Helical oligourea foldamers as powerful hydrogen bonding catalysts for enantioselective C−C bond-forming reactions. *J. Am. Chem. Soc.* **2017**, *139* (36), 12524−12532. (c) Maayan, G.; Ward, M. D.; Kirshenbaum, K. Folded biomimetic oligomers for enantioselective catalysis. *Proc. Natl. Acad. Sci. U. S. A.* **2009**, *106* (33), 13679−13684. (d) Ożga, K.; Rudzińska-Szostak, E.; Berlicki, Ł. Optimization of peptide foldamer-based artificial retro-aldolase. *Catal. Sci. Technol.* **2024**, *14* (16), 4533−4541. (e) Girvin, Z. C.; Andrews, M. K.; Liu, X.; Gellman, S. H. Foldamer-templated catalysis of macrocycle formation. *Science* **2019**, *366*, 1528−1531. (f) Prince, R. B.; Barnes, S. A.; Moore, J. S. Foldamer-based molecular recognition. *J. Am. Chem. Soc.* **2000**, *122* (12), 2758−2762. (g) Collie, G. W.; Bailly, R.; Pulka-Ziach, K.; Lombardo, C. M.; Mauran, L.; Taib-Maamar, N.; Dessolin, J.; Mackereth, C. D.; Guichard, G. Molecular recognition within the cavity of a foldamer helix bundle: encapsulation of primary alcohols in aqueous conditions. *J. Am. Chem. Soc.* **2017**, *139* (17), 6128−6137. (h) Juwarker, H.; Suk, J.; Jeong, K.-S. Foldamers with helical cavities for binding complementary guests. *Chem. Soc. Rev.* **2009**, *38* (12), 3316−3325. (i) Sobiech, T. A.; Zhong, Y.; Gong, B. Cavity-containing aromatic oligoamide foldamers and macrocycles: progress and future perspectives. *Org. Biomol. Chem.* **2022**, *20* (35), 6962−6978. (j) Zubair, I.; Martínez-Crespo, L.; Webb, S. J. Foldamer-mediated transport across phospholipid bilayers. *Curr. Opin. Chem. Biol.* **2025**, *84*, 102549. (k) Zhang, D.; Chang, W.; Shen, J.; Zeng, H. Aromatic foldamer-derived transmembrane transporters. *Chem. Commun.* **2024**, *60* (92), 13468−13491. (l) Hegedus, Z.; Grison, C. M.; Miles, J. A.; Rodriguez-Marin, S.; Warriner, S. L.;

Webb, M. E.; Wilson, A. J. A catalytic protein−proteomimetic complex: using aromatic oligoamide foldamers as activators of RNase S. *Chem. Sci.* **2019**, *10* (14), 3956−3962.
(7) (a) Wang, P. S. P.; Schepartz, A. *β*-Peptide bundles: design. build. analyze. biosynthesize. *Chem. Commun.* **2016**, *52* (47), 7420−7432. (b) Kulkarni, K.; Habila, N.; Del Borgo, M. P.; Aguilar, M.-I. Novel materials from the supramolecular self-assembly of short helical *β*3-peptide foldamers. *Front Chem.* **2019**, *7*, 70. (c) Wang, S.; Sigl, J.; Allmendinger, L.; Maurizot, V.; Huc, I. Design of an abiotic unimolecular three-helix bundle. *Chem. Sci.* **2025**, *16* (3), 1136−1146. (d) Rhys, G. G.; Wood, C. W.; Beesley, J. L.; Zaccai, N. R.; Burton, A. J.; Brady, R. L.; Thomson, A. R.; Woolfson, D. N. Navigating the structural landscape of de novo *α*-helical bundles. *J. Am. Chem. Soc.* **2019**, *141* (22), 8787−8797.
(8) Pavone, V.; Zhang, S.-Q.; Merlino, A.; Lombardi, A.; Wu, Y.; DeGrado, W. F. Crystal structure of an amphiphilic foldamer reveals a 48-mer assembly comprising a hollow truncated octahedron. *Nat. Commun.* **2014**, *5* (1), 3581.
(9) (a) Hardoin, L.; Kdouh, R.; Aidibi, Y.; Azar, S.; Siegler, B.; Allain, M.; Goeb, S.; Levillain, E.; Bouit, P.-A.; Galangau, O.; Sallé, M.; Canevet, D. Photoresponsive Helical Foldamers: Conformational Control Through Double Helix Formation and Light-Induced Protonation. *Chem. Eur. J.* **2025**, *31* (11), No. e202403771. (b) Yu, Z.; Hecht, S. Remote control over folding by light. *Chem. Commun.* **2016**, *52* (40), 6639−6653. (c) Aidibi, Y.; Azar, S.; Hardoin, L.; Voltz, M.; Goeb, S.; Allain, M.; Sallé, M.; Costil, R.; Jacquemin, D.; Feringa, B.; Canevet, D. Light- and temperature-controlled hybridization, chiral induction and handedness of helical foldamers. *Angew. Chem., Int. Ed.* **2025**, *64* (1), No. e202413629. (d) Liu, Y.; Parks, F. C.; Zhao, W.; Flood, A. H. Sequence-controlled stimuli-responsive single−double helix conversion between 1:1 and 2:2 chloride−foldamer complexes. *J. Am. Chem. Soc.* **2018**, *140* (45), 15477−15486. (e) Nagarkar, R. P.; Miller, S. E.; Zhong, S.; Pochan, D. J.; Schneider, J. P. Dynamic protein folding at the surface of stimuli-responsive peptide fibrils. *Protein Sci.* **2018**, *27* (7), 1243−1251. (f) Le Bailly, B. A. F.; Clayden, J. Dynamic foldamer chemistry. *Chem. Commun.* **2016**, *52* (27), 4852−4863. (g) Pike, S.; Telford, R.; Male, L. Reversible conformational switching of a photo-responsive ortho-azobenzene/2,6-pyridyldicarboxamide heterofoldamer. *Org. Biomol. Chem.* **2023**, *21*, 7717−7723. (h) Parks, F. C.; Liu, Y.; Debnath, S.; Stutsman, S. R.; Raghavachari, K.; Flood, A. H. Allosteric control of photofoldamers for selecting between anion regulation and double-to-single helix switching. *J. Am. Chem. Soc.* **2018**, *140* (50), 17711−17723. (i) Hua, Y.; Flood, A. H. Flipping the Switch on Chloride Concentrations with a light-active foldamer. *J. Am. Chem. Soc.* **2010**, *132* (37), 12838−12840. (j) Jeon, H.-G.; Lee, H. K.; Lee, S.; Jeong, K.-S. Foldamer-Based helicate displaying reversible switching between two distinct conformers. *Chem. Commun.* **2018**, *54*, 5740−5743. (k) Yu, Z.; Hecht, S. Remote control over folding by light. *Chem. Commun.* **2016**, *52*, 6639−6653. (l) Brioche, J.; Pike, S. J.; Tshepelevitsh, S.; Leito, I.; Morris, G. A.; Webb, S. J.; Clayden, J. Confromational Switching of a foldamer in a multicomponent system by pH-filtered selection between competing noncovalent interactions. *J. Am. Chem. Soc.* **2015**, *137*, 6680−6691.
(10) (a) Zhang, D.-W.; Zhao, X.; Hou, J.-L.; Li, Z.-T. Aromatic amide foldamers: structures, properties, and functions. *Chem. Rev.* **2012**, *112* (10), 5271−5316. (b) Gan, Q.; Wang, Y.; Jiang, H. Aromatic oligoamide foldamers: a paradigm for structure−property relationship. *Chin. Sci. Bull.* **2011**, *15* (9), 1293−1301. (c) Huc, I. Aromatic oligoamide foldamers. *Eur. J. Org. Chem.* **2004**, *2004* (1), 17−29. (d) Hill, D. J.; Mio, M. J.; Prince, R. B.; Hughes, T. H.; Moore, J. S. A field guide to foldamers. *Chem. Rev.* **2001**, *101* (12), 3893−4012. (e) Gong, B. Hollow crescents, helices, and macrocycles from enforced folding and folding-assisted macrocyclization. *Acc. Chem. Res.* **2008**, *41* (10), 1376−1386.
(11) (a) Jiang, H.; Maurizot, V.; Huc, I. Double versus single helical structures of oligopyridine-dicarboxamide strands. Part 1: Effect of oligomer length. *Tetrahedron* **2004**, *60* (44), 10029−10038. (b) Haldar, D.; Jiang, H.; Léger, J. M.; Huc, I. Double versus single helical structures of oligopyridine-dicarboxamide strands. Part 2: The role of side chains. *Tetrahedron* **2007**, *63* (27), 6322−6330. (c) Baptiste, B.; Zhu, J.; Haldar, D.; Kauffmann, B.; Léger, J.; Huc, I. Hybridization of long pyridine-dicarboxamide oligomers into multi-turn double helices: Slow strand association and dissociation, solvent dependence, and solid state structures. *Chem. Asian J.* **2010**, *5* (6), 1364−1375. (d) Shang, J.; Gan, Q.; Dawson, S. J.; Rosu, F.; Jiang, H.; Ferrand, Y.; Huc, I. Self-association of aromatic oligoamide foldamers into double helices in water. *Org. Lett.* **2014**, *16* (19), 4992−4995. (e) Ferrand, Y.; Kendhale, A. M.; Garric, J.; Kauffmann, B.; Huc, I. Parallel and antiparallel triple helices of naphthyridine oligoamides. *Angew. Chem., Int. Ed.* **2010**, *49* (10), 1778−1781. (f) Gan, Q.; Bao, C.; Kauffmann, B.; Grélard, A.; Xiang, J.; Liu, S.; Huc, I.; Jiang, H. Quadruple and double helices of 8-fluoroquinoline oligoamides. *Angew. Chem., Int. Ed.* **2008**, *47* (9), 1715−1718. (g) Berl, V.; Huc, I.; Khoury, R.; Krische, M. J.; Lehn, J.-M. Interconversion of single and double helices formed from synthetic molecular strands. *Nature* **2000**, *407*, 720−723.
(12) (a) Gan, Q.; Li, F.; Li, G.; Kauffmann, B.; Xiang, J.; Huc, I.; Jiang, H. Heteromeric double helix formation by cross-hybridization of chloro- and fluoro-substituted quinoline oligoamides. *Chem. Commun.* **2010**, *46* (2), 297−299. (b) Singleton, M. L.; Pirotte, G.; Kauffmann, B.; Ferrand, Y.; Huc, I. Increasing the size of an aromatic helical foldamer cavity by strand intercalation. *Angew. Chem., Int. Ed.* **2014**, *53* (48), 13140−13144. (c) Koehler, V.; Bruschera, G.; Merlet, E.; Mandal, P. K.; Morvan, E.; Rosu, F.; Douat, C.; Fischer, L.; Huc, I.; Ferrand, Y. High-affinity hybridization of complementary aromatic oligoamide strands in water. *Angew. Chem., Int. Ed.* **2023**, *62* (48), No. e202311639. (d) Zhan, C.; Léger, J.-M.; Huc, I. Cross-hybridization of pyridinedicarboxamide helical strands and their N-oxides. *Angew. Chem., Int. Ed.* **2006**, *45* (28), 4625−4628.
(13) (a) Qi, T.; Maurizot, V.; Noguchi, H.; Charoenraks, T.; Kauffmann, B.; Takafuji, M.; Ihara, H.; Huc, I. Solvent dependence of helix stability in aromatic oligoamide foldamers. *Chem. Commun.* **2012**, *48* (51), 6337−6339. (b) Zhao, Y.; Connor, A. L.; Sobiech, T. A.; Gong, B. Effects of oligomer length, solvents, and temperature on the self-association of aromatic oligoamide foldamers. *Org. Lett.* **2018**, *20* (17), 5486−5489. (c) Liu, R.; Connor, A. L.; Al-Mkhaizim, F. Y.; Gong, B. Aromatic oligoamides with increased backbone flexibility: Improved synthetic efficiencies, solvent-dependent folding and cooperative conformational transitions. *New J. Chem.* **2015**, *39* (5), 3217−3220. (d) Okamoto, I.; Nabeta, M.; Hayakawa, Y.; Morita, N.; Takeya, T.; Masu, H.; Azumaya, I.; Tamura, O. Acid-induced molecular folding and unfolding of N-methyl aromatic amide bearing 2,6-disubstituted pyridines. *J. Am. Chem. Soc.* **2007**, *129* (7), 1892−1893.
(14) (a) Mondal, D.; Ahmad, M.; Dey, B.; Mondal, A.; Talukdar, P. Formation of supramolecular channels by reversible unwinding-rewinding of bis(indole) double helix via ion coordination. *Nat. Commun.* **2022**, *13* (1), 6507. (b) Lee, S.; Song, G.; Jeong, K.-S. Stimuli-responsive molecular duplexes displaying duplex-to-duplex switching. *Angew. Chem., Int. Ed.* **2024**, *63*, No. e202410884.
(15) Faour, L.; Adam, C.; Gautier, C.; Goeb, S.; Allain, M.; Levillain, E.; Canevet, D.; Sallé, M. Redox-controlled hybridization of helical foldamers. *Chem. Commun.* **2019**, *55* (40), 5743−5746.
(16) (a) Zhang, A.; Ferguson, J. S.; Yamato, K.; Zheng, C.; Gong, B. Improving foldamer synthesis through protecting group induced unfolding of aromatic oligoamides. *Org. Lett.* **2006**, *8* (22), 5117−5120. (b) König, H. M.; Abbel, R.; Schollmeyer, D.; Kilbinger, A. F. M. Solid-phase synthesis of oligo(p-benzamide) foldamers. *Org. Lett.* **2006**, *8* (9), 1819−1822. (c) Yao, C.; Kauffmann, B.; Huc, I.; Ferrand, Y. Self-assembling figure-of-eight and pseudoplectoneme aromatic oligoamide ribbons. *Chem. Commun.* **2022**, *58* (38), 5789−5792. (d) Urushibara, K.; Ferrand, Y.; Liu, Z.; Masu, H.; Pophristic, V.; Tanatani, A.; Huc, I. Frustrated helicity: Joining the diverging ends of a stable aromatic amide helix to form a fluxional macrocycle. *Angew. Chem., Int. Ed.* **2018**, *57* (26), 7888−7892.
(17) Aidibi, Y.; Azar, S.; Hardoin, L.; Voltz, M.; Goeb, S.; Allain, M.; Sallé, M.; Costil, R.; Jacquemin, D.; Feringa, B.; Canevet, D. Light-

https://doi.org/10.1021/jacs.5c14812
J. Am. Chem. Soc. XXXX, XXX, XXX−XXX

and temperature-controlled hybridization, chiral induction and handedness of helical foldamers. *Angew. Chem., Int. Ed.* **2024**, *64* (1), No. e202413629.
(18) (a) Li, D.; Ma, C.; Xiang, J.; Zhang, K.; Yang, L.; Gan, Q. A disulfide switch providing absolute handedness control in double helices via conversion from the antiparallel to parallel helical pattern. *Chem. Eur. J.* **2021**, *27* (45), 11663−11669. (b) Yu, L.; Li, D.; Ma, C.; Kauffmann, B.; Liao, S.; Gan, Q. Redox-regulated and guest-driven transformations of aromatic oligoamide foldamers in advanced structures. *J. Am. Chem. Soc.* **2024**, *146* (19), 12907−12912.
(19) Kerff, F.; Liu, C.-L.; Mu, X.; Gilbert, U.; Smal, L.; Meinertzhagen, L.; Kauffmann, B.; Robeyns, K.; Singleton, M. L. Functionalized 1,8-diazaiptycenes as monomers for aromatic oligoamide foldamers. *ChemPlusChem* **2021**, *86* (8), 1162−1166.
(20) Gillis, B. T.; Hagarty, J. D. Reaction of 4-phenyl-1,2,4-triazoline-3,5-dione with conjugated dienes. *J. Org. Chem.* **1967**, *32* (2), 330−333.
(21) Berni, E.; Kauffmann, B.; Bao, C.; Lefeuvre, J.; Bassani, D. M.; Huc, I. Assessing the mechanical properties of a molecular spring. *Chem. Eur. J.* **2007**, *13* (30), 8463−8469.
(22) Řezáč, J.; Hobza, P. Advanced corrections of hydrogen bonding and dispersion for semiempirical quantum mechanical methods. *J. Chem. Theory Comput.* **2012**, *8*, 141−151.
(23) Water saturation was found to give better resolution between the resonances for the single helical and duplex forms of 2-D and 2-M, while leading to only modest differences in the association. The behavior of the oligomers towards water is described in more detail in the Supporting Information.
(24) Gole, B.; Kauffmann, B.; Tron, A.; Maurizot, V.; McClenaghan, N.; Huc, I.; Ferrand, Y. Selective and cooperative photocycloadditions within multistranded aromatic sheets. *J. Am. Chem. Soc.* **2022**, *144* (15), 6894−6906.
(25) Berl, V.; Huc, I.; Khoury, R. G.; Lehn, J.-M. Helical molecular programming: Supramolecular double helices by dimerization of helical oligopyridine-dicarboxamide strands. *Chem. Eur. J.* **2001**, *7* (13), 2810−2820.
(26) Liu, Y.-Z.; Mu, X.; Chan, C.-K.; Robeyns, K.; Wang, C.-C.; Singleton, M. L. Water binding stabilizes stacked conformations of ferrocene containing sheet-like aromatic oligoamides. *Org. Biomol. Chem.* **2021**, *19* (25), 5521−5524.

https://doi.org/10.1021/jacs.5c14812
J. Am. Chem. Soc. XXXX, XXX, XXX−XXX